

---

# SpecOffload: Unlocking Latent GPU Capacity for LLM Inference on Resource-Constrained Devices

---

Xiangwen Zhuge<sup>1</sup>, Shen Xu<sup>1</sup>, Zeyu Wang<sup>1</sup>, Fan Dang<sup>2</sup>, Xuan Ding<sup>1</sup>, Dangyang Li<sup>1</sup>,  
Yahui Han<sup>3</sup>, Tianxiang Hao<sup>1</sup>, Zheng Yang<sup>1</sup>

<sup>1</sup>Tsinghua University

<sup>2</sup>Beijing Jiaotong University

<sup>3</sup>Beijing University of Posts and Telecommunications

## Abstract

Efficient LLM inference on resource-constrained devices presents significant challenges in compute and memory utilization. Due to limited GPU memory, existing systems offload model weights to CPU memory, incurring substantial I/O overhead between the CPU and GPU. This leads to two major inefficiencies: (1) GPU cores are underutilized, often remaining idle while waiting for data to be loaded; and (2) GPU memory has a low impact on performance, as reducing its capacity has minimal effect on overall throughput. In this paper, we propose SpecOffload, a high-throughput inference engine that embeds speculative decoding into offloading. Our key idea is to unlock latent GPU resources for storing and executing a draft model used for speculative decoding, thus accelerating inference at near-zero additional cost. To support this, we carefully orchestrate the interleaved execution of target and draft models in speculative decoding within the offloading pipeline, and propose a planner to manage tensor placement and select optimal parameters. Compared with the best baseline, SpecOffload improves GPU core utilization by 4.49 $\times$  and boosts inference throughput by 2.54 $\times$ . Our code is available at <https://github.com/MobiSense/SpecOffload>.

## 1 Introduction

As Large Language Models (LLMs) evolve, their real-world use extends far beyond chatbots to diverse applications including synthetic data generation [1], form processing [2], and data wrangling [3]. These tasks are characterised by LLMs conducting offline inference in batches over a large number of tokens. For instance, corporations need to process all archives of financial documentation, whilst individuals want to construct knowledge repositories from accumulated materials. In such workloads, higher inference throughput (the number of tokens generated divided by total generation time, token/s) translates into lower total completion time, hence it is the key metric.

Privacy and cost concerns drive these tasks toward LLM deployment on edge servers or PCs, where GPU memory is a major constraint. For instance, conducting inference exclusively using GPU memory for Mixtral 8x22B (282GB) [4] requires at least four NVIDIA H100 (80GB) GPUs. Offloading is one of the mainstream solutions to memory-constrained inference, transferring most model parameters to more economical, capacious CPU memory and reloading them to GPU memory only when computation demands. There are also methods to overcome the memory bottleneck by compressing the model and KV cache, such as quantization, pruning, sparsification [5, 6, 7], etc., which are orthogonal and can be applied on top of offloading. Our focus is on designing efficient offloading strategies for high-throughput inference on resource-constrained devices.

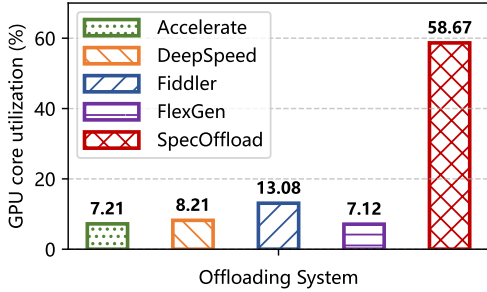


Figure 1: GPU core utilization of SOTA methods during decoding phase. Settings: Mixtral 8x7B, Env #1, SummEval dataset, details in § 5.1.

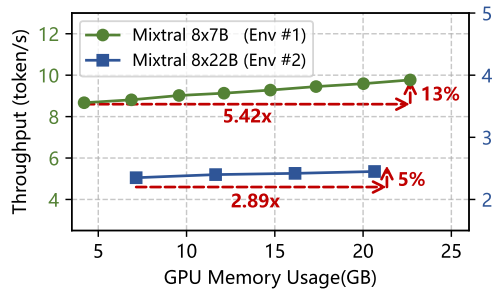


Figure 2: Impact of GPU memory on throughput during decoding phase. Settings: SummEval dataset, details in § 5.1.

However, the existing offloading work does not utilize GPU resources well. During offloading, generating each token requires reloading most model parameters from CPU memory to GPU memory for execution [8, 9, 10]. Yet I/O speeds substantially lag behind GPU computational capabilities. For instance, under typical NVIDIA RTX 4090, PCIe 4.0×16 conditions, loading a single FFN layer of the Mixtral 8×22B decoder from CPU to GPU consumes 240ms, while the actual computation on GPU requires merely 0.1ms. Consequently, total inference time is mainly determined by parameter loading time, leaving GPU resources severely underutilized.

To highlight the inefficiencies of existing approaches, we perform a detailed analysis of GPU core and memory utilization. We find that:

- **Underutilization of GPU cores.** As shown in Figure 1, during the decoding phase, the average GPU core utilization of existing methods is only 13% at most. This inefficiency stems from GPU cores frequently remaining long time idle while awaiting parameter loading. To alleviate this issue, existing methods increase the batch size to amortize I/O overhead by loading model parameters once and reusing them across the enlarged batch, thereby improving throughput [11, 10]. However, due to the limitation of GPU memory capacity or CPU computational capabilities, the scalability of the batch size remains inherently limited. The maximum batch size achieved by the SOTA scheme in Figure 1 is only 64, insufficient to bridge the huge gap between I/O and GPU latency (even with this batch size, the gap remains over 10x).
- **Marginal utility of GPU memory.** When models far exceed GPU memory capacity, throughput remains almost unchanged even when memory usage is greatly reduced during decoding phase. We conducted experiments with FlexGen [11], the most effective solution among SOTA approaches. FlexGen offloads attention computations to CPU while computing FFN layers on GPU during the decoding phase. As illustrated in Figure 2, reducing memory usage by over 5.42x for Mixtral 8×7B models led to only a 13% drop in throughput; similarly, a 2.89x reduction for Mixtral 8×22B models caused just a 5% decline. This phenomenon arises because the total volume of data to be loaded remains nearly constant, as the model size vastly exceeds the available GPU memory, leaving little room for variation even when accounting for partial parameters that can reside permanently in memory. For instance, generating a single token necessitates loading all (56) FFN layers for the leftmost blue point in Figure 2, compared to 53 layers for the rightmost blue point. Consequently, memory reduction precipitates only negligible changes in total inference time and throughput.

To harness GPU compute and memory resources more efficiently, we design SpecOffload, a novel offloading framework that unlocks latent GPU capacity by leveraging speculative decoding (SD). SD is a technique that accelerates generation by employing an auxiliary lightweight draft model to produce multiple candidate tokens, which are subsequently verified in parallel by the target model, enabling the generation of multiple tokens per forward pass [12, 13, 14].

SpecOffload embeds SD into the offloading workflow with nearly zero overhead. The key idea lies in the following two aspects:

- Computing draft model during GPU core idleness: SD requires the draft model to generate multiple candidate tokens in advance. Given the substantial idle periods prevalent in existing frameworks, these intervals can be utilized for completing the draft model’s computational tasks.

- Storing draft model uses "low-yield" GPU memory: SD requires loading a draft model into memory for draft generation. We can repurpose "low-yield" memory allocations from existing frameworks to store draft model parameters and its caches instead. For instance, as shown in [Figure 2](#), extracting 17GB of "low-yield" memory allocation provides sufficient capacity for a draft model such as Mistral 7B [\[15\]](#) to operate normally within the GPU at a small batch.

To support this, SpecOffload designs a comprehensive framework to better utilize both the computational and memory resources of the GPU. SpecOffload determines tensor distribution between GPU and CPU memory through offline Adaptive Tensor Placement ([§ 4.2](#)), dynamically schedules computational tasks via the online ParaSpec Planner ([§ 4.3](#)), and implements parallel pipelined execution of I/O and computation using the Interleaved Batch Pipeline ([§ 4.1](#)).

Our contributions are as follows:

- We conduct a quantitative analysis of GPU resource utilization in representative scenarios and identify key limitations in SOTA frameworks—underutilization of GPU cores and marginal utility of GPU memory, thus reveal a novel perspective for enhancing offloading performance.
- By designing a sub-layer model decomposition and fine-grained scheduling of compute and memory resources, we delicately embedded SD into offloading with virtually zero overhead, thereby increasing GPU core utilization by 4.49 times.
- To evaluate SpecOffload, we benchmark it against HuggingFace Accelerate [\[16\]](#), DeepSpeed-FastGen [\[8\]](#), FlexGen [\[11\]](#), and Fiddler [\[17\]](#). Results demonstrate that our system achieves throughput improvements of 4.69 $\times$ , 4.71 $\times$ , 2.54 $\times$ , and 4.04 $\times$  over these baselines, respectively.

## 2 Background and Related Work

### 2.1 Generative LLM Inference

Large language models consist of stacked Transformer layers [\[18\]](#). During inference, tokens are generated in an autoregressive paradigm: the prefill phase processes the complete input sequence to construct the KV cache, whereas in the decoding phase, subsequent token is produced based on the previously generated tokens and the cached KV states [\[19, 20, 21\]](#).

### 2.2 Speculative Decoding

Speculative decoding (SD) is a method for accelerating LLM inference. It adheres to a "Draft-then-Verify" framework: at each decoding step, a lightweight draft model initially proposes multiple candidate tokens (*e.g.*,  $(\hat{w}_1, \hat{w}_2, \hat{w}_3, \hat{w}_4)$ ), which are collectively verified by a larger target model in a single forward pass. Only the valid subset  $(w_1, w_2)$  is accepted, after which the target model resumes decoding by independently generating the subsequent token  $w_3$  [\[12, 13, 14\]](#). This approach enables the target model to generate multiple tokens per inference step. To further enhance the efficiency of SD, prior research has predominantly explored two avenues: the design of more effective draft models [\[22, 23, 24\]](#) and draft structures [\[25, 26, 27\]](#). However, traditional single-batch SD is not well-suited for integration with offloading, as the computations of the draft and target models must be executed sequentially. As a result, the GPU resources remain underutilized during the target model's verification phase. By introducing a dual-batch rotation strategy, SpecOffload enables the verifying and drafting to run concurrently, allowing SD to be seamlessly embedded into the offloading pipeline, while better utilizing GPU resources.

### 2.3 Offloading in LLM Inference

Offloading is one of the predominant solutions for enabling LLM inference under GPU memory constraints. It entails relocating certain model parameters from the expensive, limited GPU memory to the more cost-effective and abundant CPU memory [\[8, 17, 28, 29, 30, 9\]](#). I/O constraints create the primary bottleneck in offloading, as data transfer latency between CPU memory and GPU memory far exceeds the GPU's computation time. Consequently, GPU resources remain underutilized.

In throughput-oriented scenarios, existing methods typically increase the batch size to amortize I/O costs. A prevalent strategy involves altering the model's execution pattern from row-wise to column-wise, allowing each layer's parameters to be loaded once and reused across multiple batches, thereby

reducing the per-layer I/O burden [11, 10]. However, this approach is constrained by the available GPU memory and the overhead I/O of KV cache. More recent studies demonstrate that offloading attention computation to the CPU can eliminate KV cache I/O in decoding phase [31, 32, 33, 34], but in doing so, CPU compute limitations cap batch scalability. Thus, GPU resources remain significantly underutilized. In this work, by interleaving the draft model’s workload into the GPU’s idle periods between the target model’s layer-wise computations, we improve GPU core utilization by 4.49 $\times$ .

### 3 System Overview

In this work, we propose SpecOffload. As shown in Figure 3, it employs a two-phase architecture where offline tensor placement and online scheduling collectively determine a unified pipeline across GPU and CPU.

During the offline phase, the target and draft models are deployed across a heterogeneous memory hierarchy. SpecOffload automatically evaluates the hardware ecosystem, measuring CPU and GPU memory capacities, computational performance of CPU and GPU cores, and the bandwidth of data transfer channels between them. These hardware specifications, along with the configurations of models (①), are input to the Adaptive Tensor Placement (§ 4.2) to determine the initial parameter allocation strategy (②).

During the online phase, the hardware configuration and batched inputs (③) are provided to the ParaSpec Planner (§ 4.3), which, based on input length and characteristics, computes a fine-grained pipeline execution plan, including the batch sizes for target model in prefill and decoding phase, batch size for draft model, and the number of candidate tokens to generate (④).

The scheduling results from both offline and online phases (⑤,⑥) collectively determine the Interleaved Batch Pipeline (§ 4.1). The pipeline consists of three main threads: GPU computation, CPU computation, and GPU-CPU I/O. Parameter residency within GPU and CPU memory dynamically adapts in response to the progression of the I/O thread (⑦).

## 4 Method

### 4.1 Interleaved Batch Pipeline

Motivated by the differing computational demands of the prefill and decoding phases in LLM inference, we introduce the Interleaved Batch Pipeline—a phase-specific pipeline design. During the prefill stage, the target model computation dominates the GPU runtime, and we perform additional memory management before completion. In the decoding stage, we embed speculative decoding into the pipeline by finely interleaving the computations of the two models to fully utilize the GPU cores.

#### 4.1.1 Prefill Phase

While our pipeline design for the prefill phase is inspired by the "zig-zag" strategy proposed by FlexGen [11], we extend this approach by tailoring the micro-batch scheduling and parameter management to better support speculative decoding. To minimize the GPU memory footprint of the target model during the offloading stage, at the end of the prefill phase, we offload partial model parameters and the entire KV cache to CPU memory.

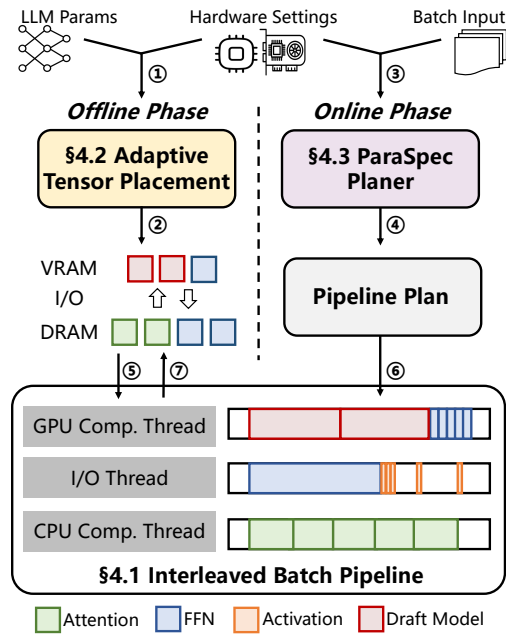


Figure 3: System overview of SpecOffload.

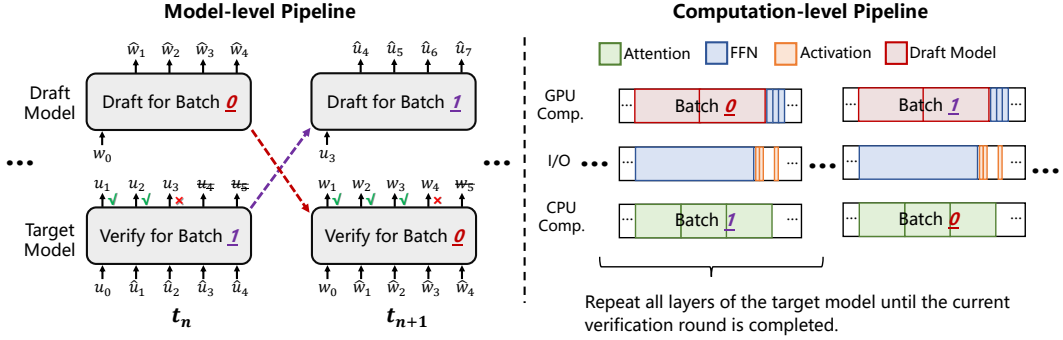


Figure 4: Schematic of the decoding pipeline. At model-level, while the target model validates Batch 1, the draft model concurrently generates tokens for Batch 0 (in time slot  $t_n$ ); the two models then alternate batches (in time slot  $t_{n+1}$ ). At computation-level, the target model’s parameters are computed layer by layer. GPU, IO, and CPU are orchestrated to perform distinct, parallelized tasks.

#### 4.1.2 Decoding Phase

During the decoding phase, we build upon the original offloading framework by repurposing the low-yield GPU memory to store the draft model and leveraging GPU idleness to execute it. To enable this, we redesign the entire pipeline at both the model and computation levels. The decoding phase pipeline is illustrated in Figure 4. In summary, our model-level design transforms conventional single-batch speculative decoding into a dual-batch interleaved scheme to facilitate parallel execution. At computation-level, the draft model’s workload is finely interleaved into the GPU idle periods between the layer-wise computations of the target model.

At model-level, the decoding phase involves two batches being processed alternately by the target and draft model. Conventional speculative decoding adopts a single-batch Draft-then-Verify paradigm, as the computations of the draft and target models must be executed sequentially. Consequently, the GPU resources left idle during the target model’s verification stage remain unused, while the system suffers from additional overhead caused by switching between models.

To overcome these limitations, we propose a dual-batch interleaved design that enables true model-level parallelism. As shown on the left side of Figure 4, in time slot  $t_n$ , while the target model verifies Batch 1, the draft model concurrently generates speculative tokens for Batch 0 ( $\hat{w}_1, \hat{w}_2, \hat{w}_3, \hat{w}_4$ ). Once both tasks are completed, the roles switch. In time slot  $t_{n+1}$ , the target model validates Batch 0 ( $w_1, w_2, w_3, w_4$ ), and the draft model proceeds with Batch 1. This alternating batch rotation continues until the generation is complete. This batch interleaving primarily enables the parallel execution of drafting and verification.

At computation-level, the decoding pipeline involves coordination among three threads: GPU computation, CPU computation, and I/O. The right side of Figure 4 provides an illustrative example. Each layer of the target model is fine-grainedly partitioned into attention and FFN components. For clarity, lightweight components such as normalization layers are omitted from the figure, as their parameter size and computational cost are negligible. As illustrated, for the majority of the inference time, the CPU performs attention computation (current batch), the system transfers same layer’s FFN parameters from CPU memory to GPU memory (current batch), and the GPU executes draft model computation (another batch), all in parallel. Upon completion of attention computation on the CPU, the intermediate activations are transferred to the GPU. Finally, once both the parameters and activations are available on the GPU, the remaining computations are quickly completed. After completing all layers of the target model (the end of a round of parallel drafting and verification at model-level), the target and draft models exchange their current batches.

Details such as where model parameters are computed, how I/O is handled, and batch configurations are determined in the § 4.2 and § 4.3.

## 4.2 Adaptive Tensor Placement

SpecOffload introduces a novel design for heterogeneous models (target and draft models), by jointly managing the parameter placement across GPU memory, CPU memory, and disk tiers, thus enabling

efficient speculative decoding. Adaptive Tensor Placement strategy intelligently assigns tensors to different memory tiers based on real-time resource availability and the current computational task, optimizing memory utilization and mitigating I/O bottlenecks.

We establish tensor prioritization hierarchically by sub-layer, categorizing based on both functional type (attention, KV cache, FFN) and computational phase. Tensors required by the current and next layers of the target model are assigned the highest priority and are preferentially placed in GPU memory. Draft model and its cache are also treated as high-priority and retained in GPU memory during decoding phase. If GPU memory capacity permits, additional parameters are pinned to further reduce I/O overhead. Remaining tensors are offloaded to CPU memory with moderate priority, leveraging its high bandwidth and low latency, as well as its ability to support certain computations. If CPU memory is exhausted, parameters are further offloaded to disk. When CPU memory is sufficient, `pin_memory()` is employed to accelerate GPU-CPU data transfer. A dynamic memory management mechanism is employed to avoid cross-tier memory swaps, ensuring that only CPU memory interfaces with both GPU memory and disk.

The core of the dynamic memory management mechanism is prefetching, which overlaps I/O with computation. For example, while computing attention of layer  $i$ , GPU memory preloads FFN of the same layer from CPU memory, and concurrently, CPU memory prefetches the parameters of layer  $i + 1$  from disk. Dedicated placeholders are reserved in GPU & CPU memory for prefetched tensors.

### 4.3 ParaSpec Planner

Interleaved Batch Pipeline section (§ 4.1) outlines our pipeline strategy; however, key parameters—such as the batch sizes of target model during prefill and decoding phase, batch size of draft model, generated draft token number, require careful tuning. To address this, we propose ParaSpec Planner, a parameter specialization module that selects optimal configurations for a given input.

**Planning Goal.** ParaSpec Planner aims to maximize model inference throughput on a given hardware configuration. Throughput is determined by two factors: the total number of tokens generated per batch inference, denoted as  $\tilde{N}_{generated}$ , and the corresponding generation latency,  $T_{generation}$ . On consumer-grade hardware, the primary system constraints lie in GPU memory capacity. Therefore, we formulate the problem as a constrained optimization task as follows:

$$\begin{aligned} \text{max } & \text{throughput} = \max \frac{\tilde{N}_{generated}}{T_{generation}} \\ \text{s.t. } & \text{gpu peak memory} \leq \text{gpu mem capacity} \end{aligned} \quad (1)$$

**Generated Tokens.** The total number of generated tokens,  $\tilde{N}_{generated}$ , is the sum of tokens  $\tilde{n}_{generated}$  produced over  $n_{iter}$  iterations for a batch of size  $bs$ . However, in our system, speculative decoding introduces randomness, causing the number of tokens generated per input in each iteration to become a random variable. We use the expected value to represent the average number of tokens that pass verification in each iteration.

$$\tilde{N}_{generated} = \sum_{bs} \sum_{n_{iter}} \tilde{n}_{generated} = bs \times n_{iter} \times \mathbb{E}[n_{generated}] \quad (2)$$

**Inference Latency.** The inference latency  $T_{generation}$  is determined by the degree of parallelism in the inference pipeline. Due to architectural differences between the prefill and decoding phases in SpecOffload, their latencies must be modeled separately,  $T_{generation} = T_{prefill} + T_{decoding}$ . Since computation in the prefill phase is primarily GPU-bound, its execution time is independent of batch size and instead depends on the number of computation steps required.

$$T_{prefill} = \left\lceil \frac{bs}{bs_{prefill}} \right\rceil \times T_{target,prefill}^{GPU} \quad (3)$$

During the decoding phase, SpecOffload performs two primary tasks: draft generation for one batch and verification for another. The overall latency is determined by the longer of the two.

$$T_{decoding} = \max(T_{target,decoding}, T_{draft}) \quad (4)$$

**Memory Constraints.** GPU memory constraints can likewise be decomposed into those for the prefill and decoding phase. In each phase, the combined memory footprint of model parameters,

intermediate activations, and KV cache must not exceed the available GPU memory. In the prefill phase, GPU memory consumption is primarily composed of two parts: the parameter size of the target model, and the KV cache required.

$$V_{prefill} = V_{target,prefill} + V_{target,KVcache} \quad (5)$$

Similarly, in decoding, GPU memory usage consists of the main model parameters, the draft model parameters, and the KV cache used by the draft model.

$$V_{decoding} = V_{target,FFN} + V_{draft} + V_{draft,KVcache} \quad (6)$$

More detailed derivations, please refer to the [Appendix A.1](#). Before using the ParaSpec Planner, a profiling program must be run on the target hardware to collect performance characteristics. However, due to the challenges of hardware measurement, OS-induced variability, and the uncertainty in draft token validity introduced by speculative decoding, such measurements may not fully reflect the actual behavior of SpecOffload during execution. Consequently, while ParaSpec Planner can produce high-quality parameter configurations, further fine-tuning may still be required to achieve optimal performance.

## 5 Evaluation

Table 1: Hardware Configurations.

	Env #1	Env #2
GPU	RTX 4090	RTX 4090
VRAM	24G	24G
PCIe	Gen3 x 16	Gen4 x 16
CPU	i9-10980XE	EPYC 7542
DRAM	256G	448G

Table 2: Dataset Configurations.

	HumanEval [35]	C-Eval [36]	SummEval [37]	SAMSum [38]
$S_{avg}$	157.54	165.46	503.02	168.10
$S_{max}$	437	483	783	1144
$S_{std}$	72.46	103.18	138.68	120.53
Task	Coding	Exam	Summarization	

### 5.1 Experimental Setup

**Implementation.** We implement SpecOffload on top of Hugging Face Transformers v4.47.1[39]. We implement pipeline using multiprocessing with shared memory for inter-process vector communication. More details is provided in [Appendix A.2](#).

**Models.** We evaluate SpecOffload using two popular and open-source models: Mixtral-8x7B [40] and Mixtral-8x22B [4]. They have 46.7B and 141B parameters in bfloat16 precision. The draft model for speculative decoding is Mistral-7B [15]. Although not evaluated, SpecOffload can support other models compatible with Transformers' model classes.

**Hardware.** We evaluate SpecOffload in two different environments, as shown in [Table 1](#). Env #2 refers to a cloud-based server.

**Datasets.** We use most common LLM benchmarks with different prompt length distributions and tasks, as shown in [Table 2](#). HumanEval dataset [35] released by OpenAI includes 164 programming problems; C-Eval dataset [36] is a comprehensive Chinese evaluation suite includes 13948 questions; SummEval dataset [37] inlcudes 100 news article from the CNN/DailyMail; SAMSum dataset [38] contains about 16k messenger-like conversations with summaries.

**Baselines.** We compare against 4 baseline systems, all designed to address GPU memory limitations.

- Hugging Face Accelerate [16] supports offloading weights of some layers based on the device map. We use its version 1.5.2. Hereinafter referred to as Accelerate.
- DeepSpeed Zero-Inference [8] supports offloading the whole weights to the CPU or disk. We use its version 0.16.1. Hereinafter referred to as DeepSpeed.
- FlexGen [11] employs a "zig-zag" inference schedule to increase throughput.
- Fiddler [17] strategically utilizes both CPU and GPU resources for MoE model inference.

Additionally, except for FlexGen, all other baselines natively support Mixtral. We adapted FlexGen to Mixtral while adhering to its original offloading strategy.

**Metrics.** Throughput (token/s) is calculated as the number of tokens generated divided by total generation time (prefill time + decoding time).

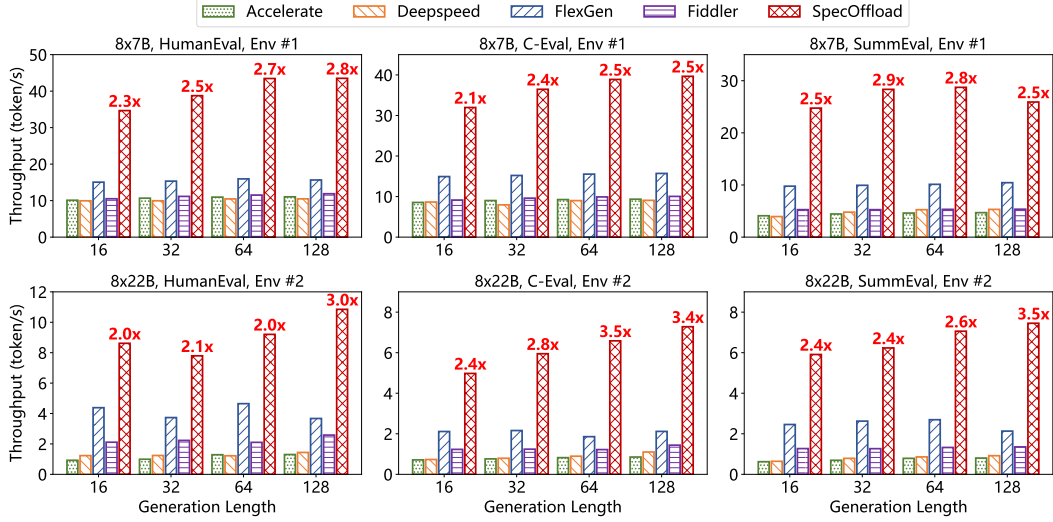


Figure 5: End-to-end comparison between SpecOffload and baselines in different scenarios.

## 5.2 End-to-end Throughput

Figure 5 illustrates the end-to-end throughput of five approaches across two environments and three datasets. In Env #1, using the Mixtral 8x7B model, SpecOffload attains an average speedup of 2.53x over the strongest baseline, FlexGen; in Env #2, with the Mixtral 8x22B model, it achieves an average speedup of 2.54x. The superior throughput of SpecOffload is attributed to the embedding of speculative decoding into the offloading pipeline. Empirical results demonstrate that computing and storing the draft model on the GPU memory confers greater performance gains than offloading either the target model’s parameters or its cache.

The performance of our method on additional datasets is provided in the [Appendix A.3.1](#). More Details on the policy setups and effective batch sizes can be found in [Appendix A.3.2](#).

## 5.3 Effectiveness Analysis

Table 3: Detail Runtime breakdown (seconds)."P" and "D" denote Prefill and Decoding, respectively. Compute(G,T) and Compute(G,D) denote the GPU computation time for the target and draft models, respectively, while Compute(C) represents the target model’s computation time on the CPU. Cache(G→C) indicates the time to transfer the KV cache from GPU memory to CPU memory.

	Phase	Total	Compute(G,T)	Compute(G,D)	Compute(C)	Weight(R)	Cache(G→C)
8x7B, Env #1	P	183.28	79.62	0	0	123.48	39.05
	D	569.21	35.34	489.02	531.23	236.2	0
8x22B, Env #2	P	280.42	42.22	0	0	166.45	91.06
	D	794.26	27.34	345.93	746.38	262.64	0

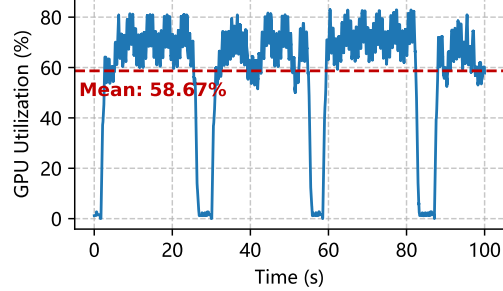
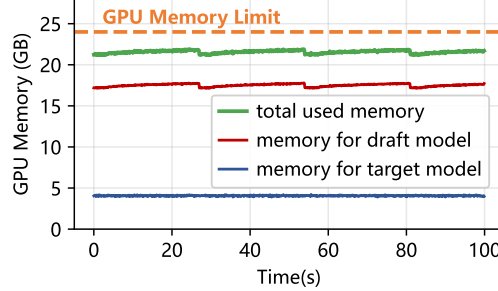


Figure 6: Decoding phase GPU core utilization.



We employ NVIDIA Nsight [41] to monitor GPU core utilization and memory consumption during the decoding phase of Mixtral 8x7B in Env #1 on the SummEval dataset. As depicted in Figure 6, the average core utilization reaches 58.67%, attains 8.14x, 7.15x, 4.49x, and 8.24x higher than Accelerate, DeepSpeed, FlexGen, and Fiddler, respectively. The elevated core utilization can be attributed to the residency of the draft model in GPU memory, enabling continuous computation.

Figure 7 reveals a periodic pattern in the draft model’s GPU memory consumption. Each cycle lasts approximately 28 seconds, characterized by a gradual increase in memory usage followed by a sharp drop and a 2-second idle window. This aligns with the behavior observed in Figure 6, where the draft model performs computation for 26 seconds and remains idle for 2 seconds awaiting the next batch. More detailed GPU memory use in Appendix A.3.3.

We show the runtime breakdown of Mixtral 8x7B in Env #1 and 8x22B in Env #2 in Table 3 on SummEval dataset. We disable overlapping and profile the time used for GPU, I/O, and CPU. Results show that our method effectively overlaps compute and I/O.

#### 5.4 Ablation Study

Table 4: Ablation study of proposed techniques on SummEval dataset. The gray tuple denotes a policy (prefill batch size, decoding batch size, draft batch size, draft max new tokens).

	All optimizations	No policy search	Serial SD	No SD
8x7B	24.743 (80, 192, 8, 8)	15.624 (50, 256, 5, 2)	17.048 (80, 192, 40, 8)	12.369 (80, 256, x, x)
8x22B	5.911 (16, 64, 8, 8)	3.486 (16, 32, 6, 6)	4.146 (16, 64, 32, 8)	1.698 (16, 80, x, x)

We then isolate the improvement brought by each individual technique. Table 4 lists the throughput SpecOffload can achieve if disabling one technique at a time. On Mixtral 8x7B, we choose target model prefill batch 80, decoding batch size of 192. And due to the design of rotating batches, the total batch size is  $192 \times 2 = 384$ . Draft model batch of 8 and generates 8 tokens per iteration. "No policy search" illustrates the performance of a random strategy, showing the importance of a good policy. We also decoupled speculative decoding from the tightly integrated pipeline into a loosely coupled serial mode. Results show that embedding speculative decoding into the pipeline is beneficial, as the naive combination of serial speculative decoding and offloading incurs additional I/O overhead from the draft model and its KV cache. Removing speculative decoding highlights its substantial performance gains. Additional ablation studies are provided in Appendix A.3.4.

#### 5.5 Load to disk

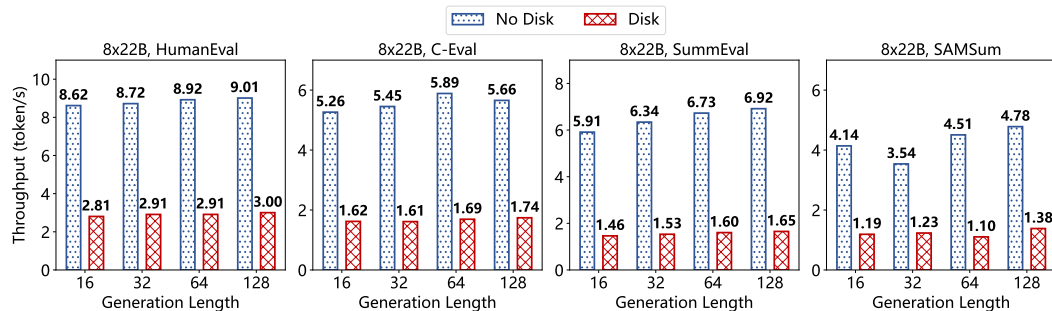


Figure 8: Throughput comparison of Mixtral 8x22B with and without disk offloading. No Disk corresponds to execution in Env #2, which has sufficient CPU memory, while Disk corresponds to execution in Env #1, where GPU memory is limited.

We further conducted experiments in Env #1 by extending the offloading to disk. The disk read and write speeds are 3.5GB/s and 1.7GB/s, respectively. Env #1 offers a memory capacity of 256GB, which is insufficient to accommodate the complete Mixtral 8x22B model (141B parameters). As shown in Figure 8, under these memory-limited conditions, load to disk SpecOffload attains 29.3% of its original throughput.

## 6 Conclusion

We identify two key inefficiencies in existing offloading frameworks for LLM inference: underutilization of GPU cores and marginal utility of GPU memory. To address these, we propose SpecOffload, which embeds speculative decoding into offloading with virtually zero overhead by leveraging idle GPU time and "low-yield" GPU memory. Experiments show up to 2.54 $\times$  throughput gains over the best baseline, demonstrating the effectiveness of our approach for high-throughput LLM inference on resource-constrained devices.

## References

- [1] Aaron Grattafiori, Abhimanyu Dubey, Abhinav Jauhri, Abhinav Pandey, Abhishek Kadian, Ahmad Al-Dahle, Aiesha Letman, Akhil Mathur, Alan Schelten, Alex Vaughan, et al. The llama 3 herd of models. *arXiv preprint arXiv:2407.21783*, 2024.
- [2] Xinyun Chen, Petros Maniatis, Rishabh Singh, Charles Sutton, Hanjun Dai, Max Lin, and Denny Zhou. Spreadsheetcoder: Formula prediction from semi-structured context. In *Proceedings of International Conference on Machine Learning*, ICML, 2021.
- [3] Avanika Narayan, Ines Chami, Laurel Orr, Simran Arora, and Christopher Ré. Can foundation models wrangle your data? *arXiv preprint arXiv:2205.09911*, 2022.
- [4] Mixtral 8x22B | Mistral AI. <https://mistral.ai/news/mixtral-8x22b>, 2024.
- [5] Raghuraman Krishnamoorthi. Quantizing deep convolutional networks for efficient inference: A whitepaper. *arXiv preprint arXiv:1806.08342*, 2018.
- [6] Jonathan Frankle and Michael Carbin. The Lottery Ticket Hypothesis: Finding Sparse, Trainable Neural Networks. In *Proceedings of International Conference on Learning Representations*, ICLR, 2018.
- [7] Song Han, Jeff Pool, John Tran, and William Dally. Learning both weights and connections for efficient neural network. In C. Cortes, N. Lawrence, D. Lee, M. Sugiyama, and R. Garnett, editors, *Proceedings of International Conference on Neural Information Processing Systems*, NIPS, 2015.
- [8] Reza Yazdani Aminabadi, Samyam Rajbhandari, Ammar Ahmad Awan, Cheng Li, Du Li, Elton Zheng, Olatunji Ruwase, Shaden Smith, Minjia Zhang, Jeff Rasley, and Yuxiong He. Deepspeed-inference: enabling efficient inference of transformer models at unprecedented scale. In *Proceedings of the International Conference on High Performance Computing, Networking, Storage and Analysis*, SC, 2022.
- [9] Artyom Eliseev and Denis Mazur. Fast inference of mixture-of-experts language models with offloading. *arXiv preprint arXiv:2312.17238*, 2023.
- [10] Zhiyuan Fang, Yuegui Huang, Zicong Hong, Yufeng Lyu, Wuhui Chen, Yue Yu, Fan Yu, and Zibin Zheng. Klotski: Efficient mixture-of-expert inference via expert-aware multi-batch pipeline. In *Proceedings of ACM International Conference on Architectural Support for Programming Languages and Operating Systems*, ASPLOS, 2025.
- [11] Ying Sheng, Lianmin Zheng, Binhang Yuan, Zhuohan Li, Max Ryabinin, Beidi Chen, Percy Liang, Christopher Ré, Ion Stoica, and Ce Zhang. Flexgen: High-throughput generative inference of large language models with a single gpu. In *Proceedings of the International Conference on Machine Learning*, ICML, 2023.
- [12] Mitchell Stern, Noam Shazeer, and Jakob Uszkoreit. Blockwise parallel decoding for deep autoregressive models. In *Proceedings of International Conference on Neural Information Processing Systems*, NIPS, 2018.
- [13] Yaniv Leviathan, Matan Kalman, and Yossi Matias. Fast inference from transformers via speculative decoding. In *Proceedings of International Conference on Machine Learning*, ICML, 2023.
- [14] Yangyi Chen, Lifan Yuan, Ganqu Cui, Zhiyuan Liu, and Heng Ji. A close look into the calibration of pre-trained language models. In *Proceedings of the Annual Meeting of the Association for Computational Linguistics*, ACL, 2023.
- [15] Albert Q. Jiang, Alexandre Sablayrolles, Arthur Mensch, Chris Bamford, Devendra Singh Chaplot, Diego de las Casas, Florian Bressand, Gianna Lengyel, Guillaume Lample, Lucile Saulnier, Lélio Renard Lavaud, Marie-Anne Lachaux, Pierre Stock, Teven Le Scao, Thibaut Lavril, Thomas Wang, Timothée Lacroix, and William El Sayed. Mistral 7B. *arXiv preprint arXiv:2310.06825*, 2023.

[16] Sylvain Gugger, Lysandre Debut, Thomas Wolf, Philipp Schmid, Zachary Mueller, Sourab Mangrulkar, Marc Sun, and Benjamin Bossan. Accelerate: Training and inference at scale made simple, efficient and adaptable. <https://github.com/huggingface/accelerate>, 2022.

[17] Keisuke Kamahori, Yile Gu, Kan Zhu, and Baris Kasikci. Fiddler: Cpu-gpu orchestration for fast inference of mixture-of-experts models. In *Proceedings of the International Conference on Learning Representations*, ICLR, 2025.

[18] Ashish Vaswani, Noam Shazeer, Niki Parmar, Jakob Uszkoreit, Llion Jones, Aidan N. Gomez, Łukasz Kaiser, and Illia Polosukhin. Attention is all you need. In *Proceedings of International Conference on Neural Information Processing Systems*, NIPS, 2017.

[19] Woosuk Kwon, Zhuohan Li, Siyuan Zhuang, Ying Sheng, Lianmin Zheng, Cody Hao Yu, Joseph Gonzalez, Hao Zhang, and Ion Stoica. Efficient memory management for large language model serving with pagedattention. In *Proceedings of Symposium on Operating Systems Principles*, SOSP, 2023.

[20] Reiner Pope, Sholto Douglas, Aakanksha Chowdhery, Jacob Devlin, James Bradbury, Jonathan Heek, Kefan Xiao, Shivani Agrawal, and Jeff Dean. Efficiently Scaling Transformer Inference. In D. Song, M. Carbin, and T. Chen, editors, *Proceedings of Machine Learning and Systems*, MLSys, 2023.

[21] Tom B. Brown, Benjamin Mann, Nick Ryder, Melanie Subbiah, Jared Kaplan, Prafulla Dhariwal, Arvind Neelakantan, Pranav Shyam, Girish Sastry, Amanda Askell, Sandhini Agarwal, Ariel Herbert-Voss, Gretchen Krueger, Tom Henighan, Rewon Child, Aditya Ramesh, Daniel M. Ziegler, Jeffrey Wu, Clemens Winter, Christopher Hesse, Mark Chen, Eric Sigler, Mateusz Litwin, Scott Gray, Benjamin Chess, Jack Clark, Christopher Berner, Sam McCandlish, Alec Radford, Ilya Sutskever, and Dario Amodei. Language models are few-shot learners. In *Proceedings of International Conference on Neural Information Processing Systems*, NIPS, 2020.

[22] Yongchao Zhou, Kaifeng Lyu, Ankit Singh Rawat, Aditya Menon, Afshin Rostamizadeh, Sanjiv Kumar, Jean-François Kagy, and Rishabh Agarwal. Distillspec: Improving speculative decoding via knowledge distillation. In *International Conference on Learning Representations*, ICLR, 2024.

[23] Jun Zhang, Jue Wang, Huan Li, Lidan Shou, Ke Chen, Gang Chen, and Sharad Mehrotra. Draft & verify: Lossless large language model acceleration via self-speculative decoding. In Lun-Wei Ku, Andre Martins, and Vivek Srikumar, editors, *Proceedings of Annual Meeting of the Association for Computational Linguistics*, ACL, 2024.

[24] Xiaoxuan Liu, Lanxiang Hu, Peter Bailis, Alvin Cheung, Zijie Deng, Ion Stoica, and Hao Zhang. Online speculative decoding. In *Proceedings of International Conference on Machine Learning*, ICML, 2024.

[25] Tianle Cai, Yuhong Li, Zhengyang Geng, Hongwu Peng, Jason D. Lee, Deming Chen, and Tri Dao. Medusa: Simple llm inference acceleration framework with multiple decoding heads. In *Proceedings of International Conference on Machine Learning*, ICML, 2024.

[26] Xupeng Miao, Gabriele Oliaro, Zhihao Zhang, Xinhao Cheng, Zeyu Wang, Zhengxin Zhang, Rae Ying Yee Wong, Alan Zhu, Lijie Yang, Xiaoxiang Shi, Chunan Shi, Zhuoming Chen, Daiyan Arfeen, Reyna Abhyankar, and Zhihao Jia. Specinfer: Accelerating large language model serving with tree-based speculative inference and verification. In *Proceedings of ACM International Conference on Architectural Support for Programming Languages and Operating Systems*, ASPLOS, 2024.

[27] Ruslan Svirchevski, Avner May, Zhuoming Chen, Beidi Chen, Zhihao Jia, and Max Ryabinin. SpecExec: Massively Parallel Speculative Decoding For Interactive LLM Inference on Consumer Devices. In *Proceedings of International Conference on Neural Information Processing Systems*, NIPS, 2024.

[28] Yixin Song, Zeyu Mi, Haotong Xie, and Haibo Chen. Powerinfer: Fast large language model serving with a consumer-grade gpu. In *Proceedings of Symposium on Operating Systems Principles*, SOSP, 2024.

[29] Leyang Xue, Yao Fu, Zhan Lu, Luo Mai, and Mahesh Marina. Moe-infinity: Activation-aware expert offloading for efficient moe serving. *arXiv e-prints arXiv:2401.14361*, 2025.

[30] Jiaao He and Jidong Zhai. Fastdecode: High-throughput gpu-efficient llm serving using heterogeneous pipelines. *arXiv e-prints arXiv:2403.11421*, 2024.

[31] Shiyi Cao, Shu Liu, Tyler Griggs, Peter Schafhalter, Xiaoxuan Liu, Ying Sheng, Joseph E. Gonzalez, Matei Zaharia, and Ion Stoica. Moe-lightning: High-throughput moe inference on memory-constrained gpus. In *Proceedings of ACM International Conference on Architectural Support for Programming Languages and Operating Systems*, ASPLOS, 2025.

[32] Xuanlin Jiang, Yang Zhou, Shiyi Cao, Ion Stoica, and Minlan Yu. Neo: Saving gpu memory crisis with cpu offloading for online llm inference. *arXiv preprint arXiv:2411.01142*, 2024.

[33] Zhao Xuanlei, Bin Jia, Haotian Zhou, Ziming Liu, Shenggan Cheng, and Yang You. HeteGen: Efficient Heterogeneous Parallel Inference for Large Language Models on Resource-Constrained Devices. In *Proceedings of Machine Learning and Systems*, MLSys, 2024.

[34] Daon Park and Bernhard Egger. Improving throughput-oriented llm inference with cpu computations. In *Proceedings of International Conference on Parallel Architectures and Compilation Techniques*, PACT, 2024.

[35] Mark Chen, Jerry Tworek, Heewoo Jun, Qiming Yuan, Henrique Ponde de Oliveira Pinto, Jared Kaplan, Harri Edwards, Yuri Burda, Nicholas Joseph, Greg Brockman, Alex Ray, Raul Puri, Gretchen Krueger, Michael Petrov, Heidy Khlaaf, Girish Sastry, Pamela Mishkin, Brooke Chan, Scott Gray, Nick Ryder, Mikhail Pavlov, Alethea Power, Lukasz Kaiser, Mohammad Bavarian, Clemens Winter, Philippe Tillet, Felipe Petroski Such, Dave Cummings, Matthias Plappert, Fotios Chantzis, Elizabeth Barnes, Ariel Herbert-Voss, William Heben Guss, Alex Nichol, Alex Paino, Nikolas Tezak, Jie Tang, Igor Babuschkin, Suchir Balaji, Shantanu Jain, William Saunders, Christopher Hesse, Andrew N. Carr, Jan Leike, Josh Achiam, Vedant Misra, Evan Morikawa, Alec Radford, Matthew Knight, Miles Brundage, Mira Murati, Katie Mayer, Peter Welinder, Bob McGrew, Dario Amodei, Sam McCandlish, Ilya Sutskever, and Wojciech Zaremba. Evaluating large language models trained on code. *arXiv preprint arXiv:2107.03374*, 2021.

[36] Yuzhen Huang, Yuzhuo Bai, Zhihao Zhu, Junlei Zhang, Jinghan Zhang, Tangjun Su, Junteng Liu, Chuancheng Lv, Yikai Zhang, Jiayi Lei, Yao Fu, Maosong Sun, and Junxian He. C-eval: A multi-level multi-discipline chinese evaluation suite for foundation models. *arXiv preprint arXiv:2305.08322*, 2023.

[37] Alexander R Fabbri, Wojciech Kryściński, Bryan McCann, Caiming Xiong, Richard Socher, and Dragomir Radev. Summeval: Re-evaluating summarization evaluation. *arXiv preprint arXiv:2007.12626*, 2020.

[38] Bogdan Gliwa, Iwona Mochol, Maciej Bieseck, and Aleksander Wawer. SAMSum corpus: A human-annotated dialogue dataset for abstractive summarization. In *Proceedings of Conference on Empirical Methods in Natural Language Processing: System Demonstrations, New Frontiers in Summarization Workshop*, EMNLP Workshop, 2019.

[39] Thomas Wolf, Lysandre Debut, Victor Sanh, Julien Chaumond, Clement Delangue, Anthony Moi, Pierrick Cistac, Tim Rault, Rémi Louf, Morgan Funtowicz, Joe Davison, Sam Shleifer, Patrick von Platen, Clara Ma, Yacine Jernite, Julien Plu, Canwen Xu, Teven Le Scao, Sylvain Gugger, Mariama Drame, Quentin Lhoest, and Alexander M. Rush. Transformers: State-of-the-art natural language processing. In *Proceedings of Conference on Empirical Methods in Natural Language Processing: System Demonstrations*, EMNLP, 2020.

[40] Albert Q Jiang, Alexandre Sablayrolles, Antoine Roux, Arthur Mensch, Blanche Savary, Chris Bamford, Devendra Singh Chaplot, Diego de las Casas, Emma Bou Hanna, Florian Bressand, et al. Mixtral of experts. *arXiv preprint arXiv:2401.04088*, 2024.

[41] NVIDIA Nsight Systems. <https://developer.nvidia.com/nsight-systems>, 2025.

## A Technical Appendices and Supplementary Material

### A.1 ParaSpec Planner

#### Planning Goal.

ParaSpec Planner aims to maximize model inference throughput on a given hardware configuration. Throughput is determined by two factors: the total number of tokens generated per batch inference, denoted as  $\tilde{N}_{generated}$ , and the corresponding generation latency,  $T_{generation}$ . On consumer-grade hardware, the primary system constraints lie in GPU memory capacity. Therefore, we formulate the problem as a constrained optimization task as follows:

$$\begin{aligned} \max \text{ throughput} &= \max \frac{\tilde{N}_{generated}}{T_{generation}} \\ \text{s.t. } \text{gpu peak memory} &\leq \text{gpu mem capacity} \end{aligned} \quad (7)$$

#### Generated Tokens.

The total number of generated tokens,  $\tilde{N}_{generated}$ , is the sum of tokens  $\tilde{n}_{generated}$  produced over  $n_{iter}$  iterations for a batch of size  $bs$ . In conventional decoding without speculation, each input generates exactly one token per iteration, making  $\tilde{n}_{generated}$  a constant. However, in our system, speculative decoding introduces randomness, causing the number of tokens generated per input in each iteration to become a random variable. As a result,  $\tilde{n}_{generated}$  cannot be expressed deterministically and is instead characterized by its expected value. Let  $\tilde{n}_{generated}$  denote the actual number of tokens generated for a single input, then  $\tilde{n}_{generated} = \mathbb{E}[n_{generated}]$ , as shown in [Equation 9](#).

$$\tilde{N}_{generated} = \sum_{bs} \sum_{n_{iter}} \tilde{n}_{generated} \quad (8)$$

$$= bs \times n_{iter} \times \mathbb{E}[n_{generated}] \quad (9)$$

To characterize the distribution of  $\tilde{n}_{generated}$ , we model the speculative decoding process. In each iteration, the draft model generates a candidate sequence of  $n_{cand}$  tokens, which is then verified by the target model. The target model returns the longest correct prefix of the candidate sequence and subsequently generates one additional correct token. The number of tokens correctly predicted by the draft model ranges from 0 to  $n_{cand}$ , so  $\tilde{n}_{generated}$  follows a distribution over the set  $\{1, \dots, n_{cand} + 1\}$ .

We assume that the probability of the draft model correctly predicting a single token is  $p$ , and that these predictions are independent across positions. Under this assumption, the probability that the main model accepts exactly  $k$  tokens is given by the probability that the first  $k - 1$  tokens are correct and the  $k$ th is incorrect, as shown in [Equation 10](#). If  $k = n_{cand} + 1$ , it corresponds to the draft model correctly predicting the entire candidate sequence, this probability distribution is formalized in [Equation 11](#).

$$\mathbb{P}[n_{generated} = k] = p^{k-1} \cdot (1 - p_{cand}), \quad k = 1, \dots, n_{cand} \quad (10)$$

$$\mathbb{P}[n_{generated} = k] = p^{k-1}, \quad k = n_{cand} + 1 \quad (11)$$

The expected value  $\mathbb{E}[n_{generated}]$  is derived in [Equation 12](#). Thus, the total number of tokens generated by the model,  $\tilde{N}_{generated}$ , is expressed as a function of  $bs$ ,  $n_{iter}$ ,  $n_{cand}$ , and  $p$ .

$$\begin{aligned} \mathbb{E}[n_{generated}] &= \sum_{k=1}^{n_{cand}+1} k \cdot \mathbb{P}[n_{generated} = k] \\ &= \frac{1}{1-p} [n_{cand}p^{n_{cand}+2} - (n_{cand} + 1)p^{n_{cand}+1} + 1] \end{aligned} \quad (12)$$

### Inference Latency.

The inference latency  $T_{\text{generation}}$  is determined by the degree of parallelism in the inference pipeline. As SpecOffload exhibits distinct behaviors in the Prefill and decoding stages, their latencies must be computed separately, in [Equation 13](#).

$$T_{\text{generation}} = T_{\text{prefill}} + T_{\text{decoding}} \quad (13)$$

In the Prefill stage, loading the full KV cache for all  $bs$  inputs would exceed GPU memory capacity. Therefore, SpecOffload partitions the batch into small Prefill batch  $bs_{\text{prefill}}$ . Since computation in the Prefill stage is primarily GPU-bound, its latency is independent of the Prefill batch size and instead determined by the number of iterations required, as formalized in [Equation 14](#).

$$T_{\text{prefill}} = \left\lceil \frac{bs}{bs_{\text{prefill}}} \right\rceil \times T_{\text{target,prefill}}^{\text{GPU}} \quad (14)$$

In each iteration, the processing time per  $bs_{\text{Prefill}}$  is primarily determined by parameter I/O ( $T_{\text{para}}^{\text{C2G}}$ ) and computation ( $T_{\text{target,comp}}^{\text{GPU}}$ ), with I/O time significantly exceeding computation time in the offloading scenario, as shown in [Equation 15](#).

$$T_{\text{target,prefill}}^{\text{GPU}} = T_{\text{para}}^{\text{C2G}} + T_{\text{target,comp}}^{\text{GPU}} \approx T_{\text{para}}^{\text{C2G}} \quad (15)$$

In the decoding stage, SpecOffload performs two primary tasks in parallel: draft generation for one batch and verification for another. The overall latency is thus determined by the slower of the two tasks in [Equation 16](#).

$$T_{\text{decoding}} = \max(T_{\text{target,decoding}}, T_{\text{draft}}) \quad (16)$$

The draft generation task incurs a latency equal to the time required to execute the draft model inference entirely on the GPU. Similarly, due to memory constraints, the draft model must also divide each batch into smaller sub-batches  $bs_{\text{draft}}$  for generation,  $T_{\text{draft}}^{\text{GPU}}$  is the time for one-batch generation. Each generation step can be further decomposed into Prefill and decoding stages, as shown in [Equation 17](#).

$$\begin{aligned} T_{\text{draft}} &= \left\lceil \frac{bs}{bs_{\text{draft}}} \right\rceil \times T_{\text{draft}}^{\text{GPU}} \\ &= \left\lceil \frac{bs}{bs_{\text{draft}}} \right\rceil \times [T_{\text{draft,prefill}}^{\text{GPU}} + (n_{\text{cand}} - 1)T_{\text{draft,decoding}}^{\text{GPU}}] \end{aligned} \quad (17)$$

For the verification task, based on SpecOffload's pipeline design, each decoder layer's FFN computation depends on both the output of the Attention module and the loading of FFN parameters. Attention computation and FFN loading are executed in parallel threads, with the completion time determined by their maximum. Subsequently, the GPU performs FFN computation, which is significantly faster than parameter loading. Therefore, its latency can be expressed as in [Equation 18](#).

$$\begin{aligned} T_{\text{target,decoding}} &= n_{\text{layer}} \times [\max(T_{\text{target,Attention}}^{\text{CPU}}, T_{\text{target,FFN}}^{\text{C2G}}) + T_{\text{target,FFN}}^{\text{GPU}}] \\ &\approx n_{\text{layer}} \times [\max(T_{\text{target,Attention}}^{\text{CPU}}, T_{\text{target,FFN}}^{\text{C2G}})] \end{aligned} \quad (18)$$

Importantly, since the Attention module is offloaded to the CPU, its runtime becomes dependent on the sub-batch size, and is modeled accordingly in [Equation 19](#).

$$T_{\text{target,Attention}}^{\text{CPU}} = n_{\text{cand}} \times bs \times t_{\text{target,Attention}}^{\text{CPU}} \quad (19)$$

### Memory constraint.

The GPU memory capacity constraint can similarly be decomposed into separate constraints for the prefill and decode phases. In both phases, the total GPU memory consumption—including model parameters, intermediate activations, and KV cache—must not exceed the available GPU memory, which directly impacts the feasible batch size per inference.

In the prefill phase, GPU memory usage primarily consists of two components: the memory footprint of the main model parameters ( $V_{\text{main}}$ ) and the KV cache required during prefill ( $V_{m, \text{KVcache}}$ ). Since the KV cache for all  $bs$  inputs would exceed GPU memory capacity, the batch is partitioned into sub-batches of size  $bs_{\text{prefill}}$ . As a result, the KV cache footprint in the prefill phase only accounts for  $bs_{\text{prefill}}$  inputs, as formalized in [Equation 20](#).

$$\begin{aligned} V_{\text{prefill}} &= V_{\text{target,prefill}} + V_{\text{target,KVcache}} \\ &= V_{\text{target,prefill}} + bs_{\text{prefill}} \times l_{\text{input}} \times v_{\text{target,KVcache}} \end{aligned} \quad (20)$$

Similarly, GPU memory usage in the decode phase consists of three components: the main model parameters loaded into GPU memory, the draft model parameters, and the KV cache used by the draft model. According to SpecOffload’s offloading strategy, only the MoE FFN parameters from the main model are loaded into GPU memory, whereas the draft model is fully resident in GPU memory. Therefore, the total GPU memory footprint during decoding is characterized in [Equation 21](#). To satisfy the memory constraint, the batch of  $bs$  inputs is partitioned into sub-batches of size  $bs_{\text{assist}}$ , as defined in [Equation 22](#).

$$V_{\text{decoding}} = V_{\text{target,FFN}} + V_{\text{draft}} + V_{\text{draft,KVcache}} \quad (21)$$

$$= V_{\text{target,FFN}} + V_{\text{draft}} + bs_{\text{draft}} \times (l_{\text{input}} + n_{\text{generated}}) \times V_{\text{draft,KVcache}} \quad (22)$$

## A.2 Implementation



Figure 9: Implementation from the perspective of Interleaved batches.

Our implementation is based on modifications to HuggingFace Transformers [39], version 4.47.1.

To implement the SpecOffload pipeline, we adopt a hybrid parallelism strategy that combines process-level and thread-level parallelism. As shown in Figure 9, the input sequence is split into two interleaved batches, which alternate between draft generation and large-model verification. Each batch is processed on a separate thread, with synchronization managed via inter-thread events. After completing its generation and verification task in each iteration, a thread signals its completion and waits for the other thread to do the same. The next iteration begins only after both threads have finished the current one. This design enables parallel execution of Batch 0’s draft generation and Batch 1’s verification. However, from the perspective of a single batch (Batch 0 or Batch 1), the draft and verify stages remain sequential.

In this design, the draft model performs full-sequence autoregressive inference on GPU during the generation stage, while the large model remains computing on CPU to avoid resource contention. Given that the draft model executes strictly in a sequential manner—processing only one batch at any time—parallel instantiation is unnecessary. To further minimize GPU memory consumption, only a single copy of the draft model is loaded and isolated within a dedicated auxiliary process. Communication between this draft model process and the main process hosting the large model is established via shared memory, enabling low-latency data transfer, while inter-process events are employed to enforce strict execution ordering and synchronization.

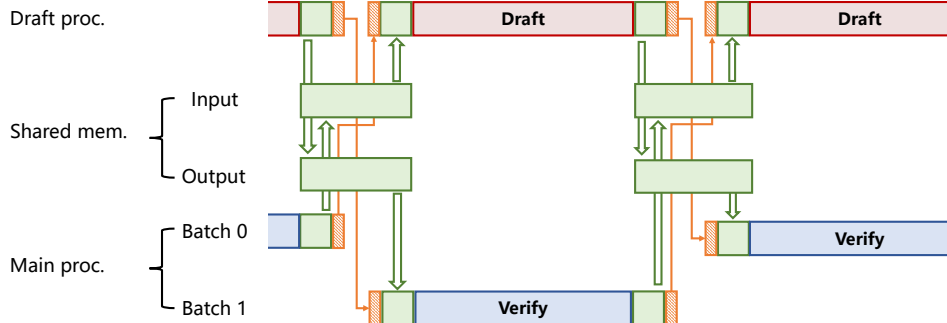


Figure 10: Inter-process communication diagram. Orange blocks represent the send/receive modules within each process, while green blocks indicate the inter-process communication modules. "Input" and "Output" are defined with respect to the Draft process.

As shown in Figure 10, inter-process communication is centered around two shared memory regions, with tokens as the primary data exchanged. The Draft process writes generated draft tokens to the output shared memory for consumption by the Main process, and reads verified tokens from the input shared memory region. When a thread in the Main process reaches the verify stage and requires draft tokens, it waits for the draft model to signal availability, then reads from shared memory. Upon finishing computation, the draft model signals completion and readiness for the next task using event flags, ensuring proper synchronization and preventing data races or overlap between batches. This tightly coordinated mechanism enables efficient and orderly pipelined execution across model components, while keeping both memory footprint and runtime overhead to a minimum.

### A.3 Additional Experimental Results

#### A.3.1 End-to-end Throughput

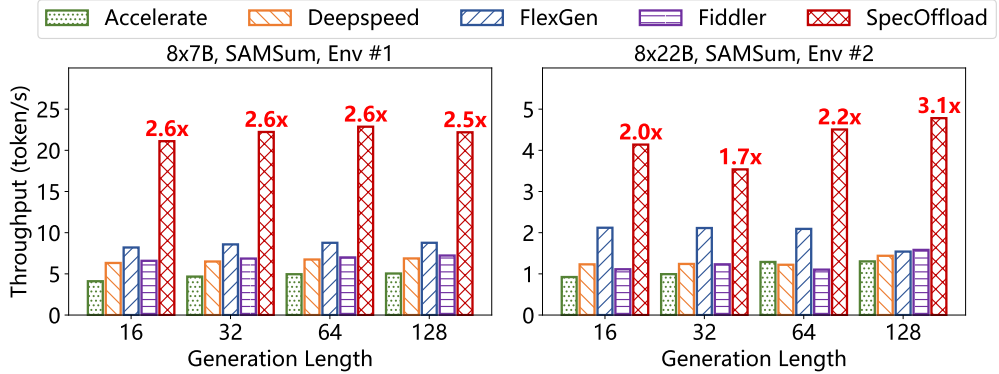


Figure 11: End-to-end comparison between SpecOffload and baselines on SAMSum.

In addition to the datasets discussed in the main text, we further evaluated SpecOffload on the SAMSum dataset [38], which has an average input length of 168.1 and a maximum length of 1144. The SAMSum dataset contains about 16k messenger-like conversations with summaries. The results on SAMSum are consistent with those observed on the other datasets. As shown in Figure 11, SpecOffload achieves a throughput of 2.575 $\times$  that of the best baseline on the Mixtral 8 $\times$ 7B model, and 2.25 $\times$  on the Mixtral 8 $\times$ 22B model.

#### A.3.2 Impact of Policy

We present detailed end-to-end throughput data, as shown in Table 5, Table 6, Table 7, Table 8, Table 9, and Table 10, to simulate different scenarios and analyze the impacts of policy on throughput by generating 16 tokens. Due to the large number of GPU hours required to complete all (prefill batch size, decoding batch size, draft batch size, draft max new tokens) combinations using Mixtral 8 $\times$ 22B in Env #2, we evaluated only a subset of possible configurations.

The prefill batch size is a tunable parameter for which the optimal value can be explicitly determined by the scheduling algorithm, as the Prefill stage does not involve speculative decoding and thus is free from probabilistic uncertainty. Under the experimental setup of Table 7, the optimal value is 80. For example, comparing entries 5 and 27 in Table 7—where all other parameters are held constant—the higher throughput of entry 27 is attributed to its more optimal Prefill batch size.

The decoding batch size and draft max new tokens jointly affect the verification latency of the target model. Since the target model’s computation is offloaded to the CPU, the speculative decoding verification cannot achieve the same level of tight serialization as on the GPU. As a result, increasing the batch size or the number of new tokens leads to longer CPU computation time. As illustrated by entries 26–30 and 10, 20, 30, 40 in Table 7, neither a larger batch size nor a higher max new token value consistently yields better performance.

The decoding batch size, draft batch size, and draft max new tokens jointly impact the generation latency of the draft model. Due to GPU memory constraints, the draft batch size is typically limited to a small value. However, since all draft model computations are executed on the GPU, they are highly efficient. This allows the full decoding batch to be processed through a fine-grained, multi-round strategy. As long as the draft model’s token generation time remains below the I/O-bound latency, it does not constitute a performance bottleneck.

The results in Table 10 exhibit a similar pattern. These four parameters are tightly coupled and collectively determine the overall system throughput. Given that our design introduces at least four tunable parameters, finding optimal settings through enumeration or heuristics alone is highly unlikely. This highlights the critical role of the Paraspec Planner in the overall system.

Table 5: Impact of policy on Mixtral 8x7B in Env #1, HumanEval dataset.

No.	Prefill Batch Size	Decoding Batch Size	Draft batch size	Draft max new token	Throughput (token/s)
1	80	200	10	8	<b>32.821</b>
2	80	160	6	1	<b>15.869</b>
3	80	160	6	2	<b>20.964</b>
4	80	160	6	4	<b>28.914</b>
5	80	160	6	6	<b>33.711</b>
6	80	160	6	8	<b>33.690</b>
7	80	160	8	1	<b>15.834</b>
8	80	160	8	2	<b>20.940</b>
9	80	160	8	4	<b>29.267</b>
10	80	160	8	6	<b>32.520</b>
11	80	160	8	8	<b>32.776</b>
12	80	160	10	1	<b>15.835</b>
13	80	160	10	2	<b>21.120</b>
14	80	160	10	4	<b>29.499</b>
15	80	160	10	6	<b>32.226</b>
16	80	160	10	8	<b>32.540</b>
17	80	200	6	1	<b>18.736</b>
18	80	200	6	2	<b>24.737</b>
19	80	200	6	4	<b>29.091</b>
20	80	200	6	6	<b>31.641</b>
21	80	200	6	8	<b>33.014</b>
22	80	200	8	1	<b>18.828</b>
23	80	200	8	2	<b>24.813</b>
24	80	200	8	4	<b>30.452</b>
25	80	200	8	6	<b>32.649</b>
26	80	200	8	8	<b>31.884</b>
27	80	200	10	1	<b>18.865</b>
28	80	200	10	2	<b>24.675</b>
29	80	200	10	4	<b>30.363</b>
30	80	200	10	6	<b>32.716</b>
31	80	200	10	8	<b>33.072</b>
32	80	256	6	1	<b>21.166</b>
33	80	256	6	2	<b>26.052</b>
34	80	256	6	4	<b>30.279</b>
35	80	256	6	6	<b>32.325</b>
36	80	256	6	8	<b>32.812</b>
37	80	256	8	1	<b>20.683</b>
38	80	256	8	2	<b>27.123</b>
39	80	256	8	4	<b>31.829</b>
40	80	256	8	6	<b>33.622</b>
41	80	256	8	8	<b>33.247</b>
42	80	256	10	1	<b>20.546</b>
43	80	256	10	2	<b>26.987</b>
44	80	256	10	4	<b>30.679</b>
45	80	256	10	6	<b>34.665</b>
46	80	256	10	8	<b>33.445</b>

Table 6: Impact of policy on Mixtral 8x7B in Env #1, C-Eval dataset.

No.	Prefill Batch Size	Decoding Batch Size	Draft batch size	Draft max new token	Throughput (token/s)
1	96	256	8	4	<b>26.489</b>
2	96	288	8	4	<b>28.449</b>
3	96	300	8	4	<b>28.209</b>
4	96	256	6	2	<b>25.363</b>
5	96	256	6	4	<b>27.823</b>
6	96	256	6	6	<b>28.712</b>
7	96	256	6	8	<b>28.531</b>
8	96	256	8	2	<b>25.347</b>
9	96	256	8	4	<b>27.449</b>
10	96	288	6	2	<b>25.254</b>
11	96	288	6	4	<b>28.685</b>
12	96	288	6	6	<b>29.199</b>
13	96	288	6	8	<b>29.385</b>
14	96	288	8	2	<b>26.126</b>
15	96	288	8	4	<b>28.679</b>
16	96	288	8	6	<b>29.329</b>
17	96	300	6	2	<b>24.821</b>
18	96	300	6	4	<b>28.240</b>
19	96	300	6	6	<b>29.134</b>
20	96	300	6	8	<b>30.781</b>
21	96	300	8	2	<b>26.268</b>
22	96	300	8	4	<b>30.652</b>
23	96	300	8	6	<b>31.968</b>

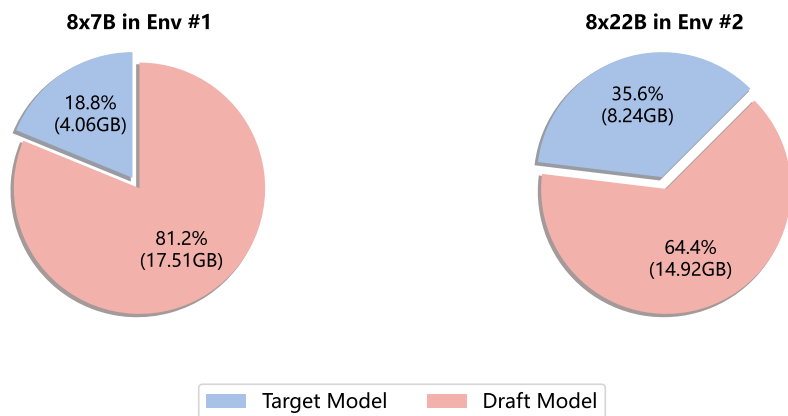


Figure 12: GPU Memory Allocation Overview.

Table 7: Impact of policy on Mixtral 8x7B in Env #1, SummEval dataset.

No.	Prefill Batch Size	Decoding Batch Size	Draft batch size	Draft max new token	Throughput (token/s)
1	50	128	5	5	<b>18.937</b>
2	50	128	5	3	<b>19.735</b>
3	50	256	5	5	<b>19.890</b>
4	50	256	5	3	<b>17.560</b>
5	50	256	5	2	<b>15.624</b>
6	80	128	5	1	<b>11.682</b>
7	80	128	5	2	<b>14.509</b>
8	80	128	5	4	<b>19.464</b>
9	80	128	5	6	<b>21.166</b>
10	80	128	5	8	<b>21.531</b>
11	80	128	8	1	<b>11.629</b>
12	80	128	8	2	<b>14.408</b>
13	80	128	8	4	<b>18.321</b>
14	80	128	8	6	<b>16.989</b>
15	80	128	8	8	<b>21.958</b>
16	80	192	5	1	<b>14.764</b>
17	80	192	5	2	<b>16.830</b>
18	80	192	5	4	<b>21.072</b>
19	80	192	5	6	<b>22.029</b>
20	80	192	5	8	<b>22.712</b>
21	80	192	8	1	<b>14.305</b>
22	80	192	8	2	<b>16.757</b>
23	80	192	8	4	<b>21.435</b>
24	80	192	8	6	<b>23.653</b>
25	80	192	8	8	<b>24.732</b>
26	80	256	5	1	<b>14.809</b>
27	80	256	5	2	<b>16.781</b>
28	80	256	5	4	<b>20.441</b>
29	80	256	5	6	<b>21.841</b>
30	80	256	5	8	<b>21.741</b>
31	80	256	8	1	<b>13.822</b>
32	80	256	8	2	<b>16.265</b>
33	80	256	8	4	<b>17.243</b>
34	80	256	8	6	<b>12.903</b>
35	80	256	8	8	<b>11.103</b>
36	80	320	5	1	<b>4.444</b>
37	80	320	5	2	<b>5.757</b>
38	80	320	5	4	<b>7.761</b>
39	80	320	5	6	<b>12.376</b>
40	80	320	5	8	<b>11.503</b>
41	80	320	8	1	<b>4.550</b>
42	80	320	8	2	<b>6.074</b>
43	80	320	8	4	<b>11.785</b>
44	80	320	8	6	<b>13.218</b>
45	80	320	8	8	<b>11.293</b>

Table 8: Impact of policy on Mixtral 8x22B in Env #2, HumanEval dataset.

No.	Prefill Batch Size	Decoding Batch Size	Draft batch size	Draft max new token	Throughput (token/s)
1	32	128	4	4	<b>7.112</b>
2	32	128	4	6	<b>7.921</b>
3	32	128	4	8	<b>7.564</b>
4	32	128	6	4	<b>8.617</b>
5	32	128	6	6	<b>7.901</b>
6	32	128	6	8	<b>7.155</b>
7	32	128	8	4	<b>6.599</b>
8	32	128	8	6	<b>7.913</b>
9	32	128	8	8	<b>7.677</b>
10	32	192	4	4	<b>7.291</b>
11	32	192	4	6	<b>7.083</b>
12	32	192	4	8	<b>4.874</b>
13	32	192	6	4	<b>7.753</b>
14	32	192	6	4	<b>7.733</b>
15	32	192	6	6	<b>7.578</b>
16	32	192	6	8	<b>4.510</b>
17	32	192	8	4	<b>8.536</b>
18	32	192	8	6	<b>6.574</b>

Table 9: Impact of policy on Mixtral 8x22B in Env #2, C-Eval dataset.

No.	Prefill Batch Size	Decoding Batch Size	Draft batch size	Draft max new token	Throughput (token/s)
1	16	32	6	4	<b>3.430</b>
2	16	32	6	6	<b>4.510</b>
3	16	32	6	8	<b>4.321</b>
4	16	32	8	4	<b>3.607</b>
5	16	32	8	6	<b>4.230</b>
6	16	32	8	8	<b>4.742</b>
7	32	32	6	4	<b>3.726</b>
8	32	32	6	6	<b>4.977</b>
9	32	32	6	8	<b>4.513</b>
10	32	32	8	4	<b>3.969</b>
11	32	32	8	6	<b>4.233</b>
12	32	32	8	8	<b>3.894</b>
13	32	32	6	4	<b>3.543</b>
14	32	32	6	6	<b>4.647</b>
15	32	32	6	8	<b>4.063</b>
16	32	32	8	4	<b>4.030</b>
17	32	32	8	6	<b>4.231</b>
18	32	32	8	8	<b>3.609</b>
19	16	64	6	4	<b>4.160</b>
20	16	64	6	6	<b>4.510</b>
21	16	64	6	8	<b>3.915</b>
22	16	64	8	4	<b>3.588</b>

Table 10: Impact of policy on Mixtral 8x22B in Env #2, SummEval dataset.

No.	Prefill Batch Size	Decoding Batch Size	Draft batch size	Draft max new token	Throughput (token/s)
1	16	64	6	4	<b>4.579</b>
2	16	32	6	4	<b>3.711</b>
3	16	32	6	6	<b>3.486</b>
4	16	32	6	8	<b>4.225</b>
5	16	32	8	4	<b>3.862</b>
6	16	32	8	6	<b>3.998</b>
7	16	32	8	8	<b>3.975</b>
8	16	64	6	4	<b>4.529</b>
9	16	64	6	6	<b>5.141</b>
10	16	64	6	8	<b>4.977</b>
11	16	64	8	4	<b>4.546</b>
12	16	64	8	6	<b>4.590</b>
13	16	64	8	8	<b>5.911</b>

### A.3.3 GPU Memory Usage

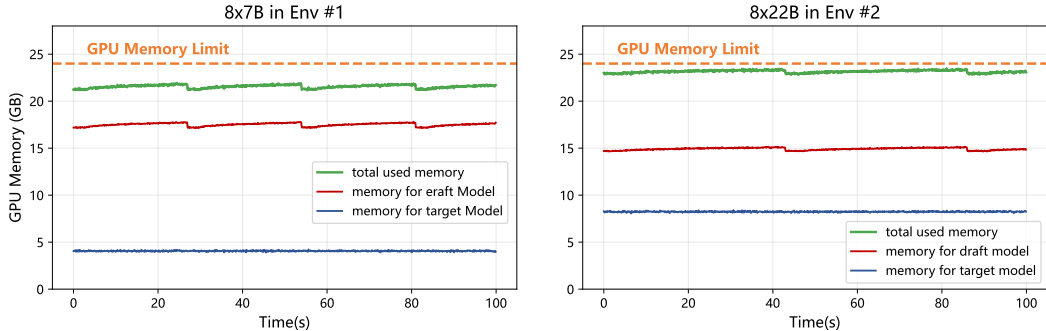


Figure 13: Runtime GPU Memory Monitoring.

We used NVIDIA Nsight [41] to monitor runtime GPU memory usage on the SummEval dataset. As shown in Figure 12, only the parameters essential for target model offloading are retained in memory, while the remaining space is occupied by the draft model and its cache. This aligns with our design rationale: during offloading, it is more efficient to allocate GPU memory to the draft model rather than storing the target model parameters.

Runtime GPU memory monitoring reveals a periodic pattern in the draft model's memory usage. As shown in the left panel of Figure 13, each cycle lasts approximately 28 seconds, characterized by a gradual increase in memory usage followed by a sharp drop and a 2-second idle window. This aligns with the behavior observed in Figure 6, where the draft model performs computation for 26 seconds and remains idle for 2 seconds awaiting the next batch.

### A.3.4 Ablation Study

In addition to the main results, we conducted ablation studies on other datasets. The results are as follows:

Table 11: Ablation study of proposed techniques on HumanEval dataset. The gray tuple denotes a policy (Prefill batch size, decoding batch size, draft batch size, draft max new tokens).

	All optimizations	No policy search	Serial SD	No SD
8x7B	34.665 (80, 256, 10, 6)	15.869 (80, 160, 6, 1)	15.005 (80, 256, 32, 6)	16.468 (80, 192, x, x)
8x22B	8.617 (32, 128, 6, 4)	4.510 (32, 192, 6, 8)	5.264 (32, 128, 32, 8)	4.108 (16, 64, x, x)

Table 12: Ablation study of proposed techniques on C-Eval dataset. The gray tuple denotes a policy (Prefill batch size, decoding batch size, draft batch size, draft max new tokens).

	All optimizations	No policy search	Serial SD	No SD
8x7B	31.968 (96, 300, 8, 6)	26.126 (96, 288, 8, 2)	21.989 (96, 288, 24, 6)	15.106 (96, 288, x, x)
8x22B	4.977 (32, 32, 6, 6)	3.588 (16, 64, 8, 4)	3.820 (32, 64, 16, 6)	1.812 (32, 64, x, x)

Table 13: Ablation study of proposed techniques on SAMSum dataset. The gray tuple denotes a policy (Prefill batch size, decoding batch size, draft batch size, draft max new tokens).

	All optimizations	No policy search	Serial SD	No SD
8x7B	21.109 (100, 300, 6, 4)	12.694 (80, 256, 8, 2)	13.64 (100, 300, 24, 4)	13.072 (80, 256, x, x)
8x22B	4.139 (16, 64, 8, 6)	3.059 (16, 64, 6, 4)	3.544 (16, 64, 16, 6)	2.378 (16, 80, x, x)

#### A.4 Limitation

The main limitation of this paper lies in the fact that speculative decoding is not a consistently reliable method for acceleration. In extreme cases, none of the draft tokens in multiple batches may be accepted, which greatly limits the acceleration effect of SpecOffload.